ADVANCED MATERIALS
www.advmat.de

Unveiling Energy Loss Mechanisms to Empower Ternary Organic Solar Cells with over 20% Efficiency: A Systematic Oligomeric Approach

Hao Xia, Caifa You, Jiehao Fu, Dou Luo, Ruijie Ma, Heng Liu, Yongwen Lang, Xinhui Lu, Weiguo Zhu,* and Gang Li**

In organic solar cells (OSCs), the ternary strategy is a mainstream approach to obtaining highly efficient OSCs. A deeper understanding of working mechanisms and the material selection criteria for boosting open-circuit voltage (V_{OC}) is essential for further OSC breakthrough. Through a modular design principle, a series of oligomeric donors – 5BDD, 5BDD-F, 5BDT-F, and 5BDT-Cl – with similar molecular configurations but varying HOMO levels is systematically designed. These findings reveal that the HOMO levels of these oligomers have a negligible impact on the V_{OC} of the ternary OSCs. Instead, their excellent compatibility with acceptors played a pivotal role in enhancing V_{OC}. The oligomers effectively suppressed excessive acceptor aggregation and achieved Aggregation-Caused Quenching Suppression (ACQS), strengthening the external electroluminescence quantum efficiency (EQE_{EL}) and reducing non-radiative recombination energy losses. Simultaneously, oligomers fine-tuned and optimized the morphology of the blend films, leading to a higher fill factor (FF) and improved performance. Notably, the 5BDT-F- and 5BDT-Cl-based ternary OSCs achieved impressive power conversion efficiencies (PCEs) of 19.8% and 20.1% (certified 19.76%), with FFs of 80.9% and 80.7%, respectively. This work elucidates the unusual role of the third component energy levels on the V_{OC} in ternary OSCs and offers valuable guidance for future OSC design.

1. Introduction

Photovoltaic (PV) technology is rapidly evolving due to the characteristics of abundant, clean, and sustainable exploitability of solar energy.[1–4] Among these, organic solar cell (OSC) technology has garnered considerable attention and research due to its low cost, light weight, flexibility, translucency, and roll-to-roll fabrication capabilities.[5,6] One of the main challenges of OSCs is their relatively low power conversion efficiency (PCE) compared to inorganic solar cells and perovskite solar cells.[7,8] However, to further enhance the performance of OSCs, particularly the V_{OC}, researchers have explored various strategies.[9–14] Among these, the ternary strategy, which involves incorporating a third component into the binary blend of donor and acceptor, has emerged as a promising approach.[12–14]

The ternary strategy offers several advantages. It allows for fine-tuning of the absorption spectrum, enabling better light harvesting and improving the overall PCE.[15–17] Additionally, the introduction of a third component can modulate the energy levels and morphology of the active layer, which are critical for optimizing charge generation, transport, and collection.[18–20] However, implementing the ternary strategy is still unclear, with many challenges. One of the primary difficulties lies in ensuring the suitable compatibility of the third component with the primary donor and acceptor materials.[21–23] Poor compatibility

H. Xia, J. Fu, R. Ma, Y. Lang, G. Li
Department of Electrical and Electronic Engineering
Research Institute of Smart Energy (RISE)
Photonic Research Institute (PRI)
The Hong Kong Polytechnic University
Hung Hum Kowloon
Hong Kong 999077, P. R. China
E-mail: jiehaojh.fu@polyu.edu.hk; gang.w.li@polyu.edu.hk

The ORCID identification number(s) for the author(s) of this article can be found under https://doi.org/10.1002/adma.202501428

DOI: 10.1002/adma.202501428

H. Xia, W. Zhu
School of Materials Science and Engineering
Jiangsu Engineering Research Center of Light-Electricity-Heat Energy-Converting Materials and Applications
Jiangsu Collaborative Innovation Center of Photovoltaic Science and Engineering
Changzhou University
Changzhou 213164, P. R. China
E-mail: zwg@cczu.edu.cn

C. You
Center for AIE Research
Guangdong Provincial Key Laboratory of New Energy Materials Service Safety
College of Materials Science and Engineering
Shenzhen University
Shenzhen 518060, P. R. China

can result in severe phase separation, excessive aggregation, and hindered exciton dissociation.[24–26] On the other hand, overly high compatibility can lead to difficulties in phase separation, impaired charge transport, and increased charge recombination, all of which negatively impact device performance.[27–29] Therefore, the rational design of the third component with optimal donor-acceptor compatibility, along with achieving the desired active layer morphology, is crucial for developing high-performance ternary devices. Moreover, understanding the energy loss mechanisms in ternary OSCs is essential for optimizing their performance. However, ternary systems add complexity, as the third component could unpredictably alter the morphology and electronic properties of the active layer.[30–32] Moreover, it is often observed that the energy level of the third component affects the V_{OC} loss in ternary OSCs, but it is tightly coupled with morphology modification and the underlying mechanism behind this influence remains unclear.[33–35] Typically, when the third component is a donor or acceptor, molecules with deeper HOMO levels than the host donor or higher LUMO levels than the host acceptor are chosen to construct ternary OSCs to enhance the device's V_{OC}. For instance, Zhang et al. introduced the S3 polymer, with a deeper HOMO level, into the PM6:Y6 system, increasing the V_{OC} from 0.844 to 0.856 V.[32] Similarly, Gao et al. used the small molecule ZW1, which has a deep HOMO level, as the third component in the D18:Y6 system, boosting the V_{OC} from 0.848 to 0.860 V.[33] However, in our previous research, we discovered that even selecting oligomer donors with higher HOMO levels than PM6 as the third component still improved the V_{OC}.[34,35] This finding challenges the conventional understanding.

Our research aims to elucidate the underlying mechanism behind this phenomenon by systematically investigating the effect of oligomeric donor materials with varying HOMO levels on the V_{OC} of ternary OSCs. We synthesized a series of oligomers (5BDD, 5BDD-F, 5BDT-F, 5BDT-Cl, **Figure 1**) with HOMO levels spanning both above and below that of the primary donor, PM6, by modularly combining BDD and BDT units with F or Cl substitutions. Through this straightforward design, our results unexpectedly showed that the introduction of these oligomers consistently improved the V_{OC} of the ternary devices, regardless of the oligomer's HOMO level. The V_{OC} of PM6:5BDD:BO-4Cl, PM6:5BDD-F:BO-4Cl PM6:BDT-F:BO-4Cl and PM6:5BDT-Cl:BO-4Cl are 0.843, 0.844, 0.847, and 0.848 V, respectively, which are higher than that of control (0.833 V). This finding challenges the conventional understanding of the role of HOMO levels in determining V_{OC}. We further found that the improved V_{OC} was due to the excellent compatibility between the oligomers and the acceptor, which suppressed excessive aggregation and achieved ACQS effects, enhancing EQE_{EL} and minimizing nonradiative energy loss. Additionally, the precise morphological tuning improved the FF, and the V_{OC} enhancement contributed by the oligomers resulted in optimal performance for PM6:5BDT-F:BTP-eC9 and PM6:5BDT-Cl:BTP-eC9 ternary OSCs, achieving excellent PCEs of 19.8% and 20.1% (certified 19.76%), respectively, representing state-of-the-art performance in OSCs. Our study demonstrates that in ternary OSCs, the compatibility of the third component has a more significant impact on V_{OC} than its HOMO level. This finding offers new insights into the energy loss mechanisms in ternary OSCs and underscores the importance of selecting compatible materials to achieve high-performance devices.

2. Results and Discussion

2.1. Synthesis, Optical, and Electrochemical Properties

The synthesis routes for 5BDT-F and 5BDT-Cl are outlined in **Scheme 1**. The synthesis procedures for 5BDD and 5BDD-F are available in previous literature sources.[35,36] Compounds 1 and 4 were obtained from a commercial supplier (Nanjing Zhiyan Technology Co., Ltd). Compound 1 was reacted with varying equivalents of trimethyl-tin chloride to produce compounds 2 and 3. Compound 5 was synthesized by reacting compound 2 with compound 4 via a Stille single coupling reaction. Finally, compound 3 was reacted with compound 5 through a Stille double coupling reaction to yield the target molecule 5BDT-F and 5BDT-Cl. Detailed synthetic procedures are provided in the Electronic Supporting Information (ESI). The structures of all products were confirmed by ^{1}H-NMR spectroscopy. Additionally, ^{13}C-NMR and MALDI-TOF mass spectrometry were used to verify the structures of 5BDT-F and 5BDT-Cl. Compounds 5BDD, 5BDD-F, 5BDT-F, and 5BDT-Cl exhibited excellent solubility in common solvents such as dichloromethane (DCM), chloroform (CF), chlorobenzene (CB), and o-xylene (O-XY).

The optical properties of 5BDD, 5BDD-F, 5BDT-F, 5BDT-Cl, PM6, and BO-4Cl were investigated through UV–vis absorption spectra in thin films (Figure 1b), with the corresponding optical data summarized in **Table 1**. All oligomer films exhibit broad absorption in the 450–700 nm range, effectively complementing the absorption profile of BO-4Cl. Compared to PM6, these oligomers show a slight blue shift in absorption. Their optical bandgaps (E_g^{opt}) were calculated to be 1.87, 1.88, 1.92, and 1.93 eV, respectively. The distinct absorption shoulders in the oligomer films suggest good π–π stacking.[37] Additionally, we measured the absorption of the blend films, as shown in Figure S1b (Supporting Information). It can be observed that the absorption intensity of both the donor and acceptor components in the ternary blend films has increased, which is beneficial for enhancing the J_{SC}. In addition, the absorption of BO-4Cl neat film as well as BO-4Cl:10% oligomer blend films were also studied (Figure S1c,d, Supporting Information). It was found that there was a slight blue shift in the absorption of the blend films compared to the pure BO-4Cl. This may be due to the inhibition of BO-4Cl aggregation by the addition of oligomers. The electrochemical properties of the oligomers were determined by cyclic voltammetry (CV) (Figure S2, Supporting Information). The HOMO levels of 5BDT-F and 5BDT-Cl were calculated from the onset oxidation potentials using an empirical equation, resulting in values of

D. Luo
Department of Applied Biology and Chemical Technology and Research Institute for Smart Energy
The Hong Kong Polytechnic University
Hung Hom, Hong Kong 999077, P. R. China
H. Liu, X. Lu
Department of Physics
The Chinese University of Hong Kong
New Territories, Hong Kong 999077, P. R. China

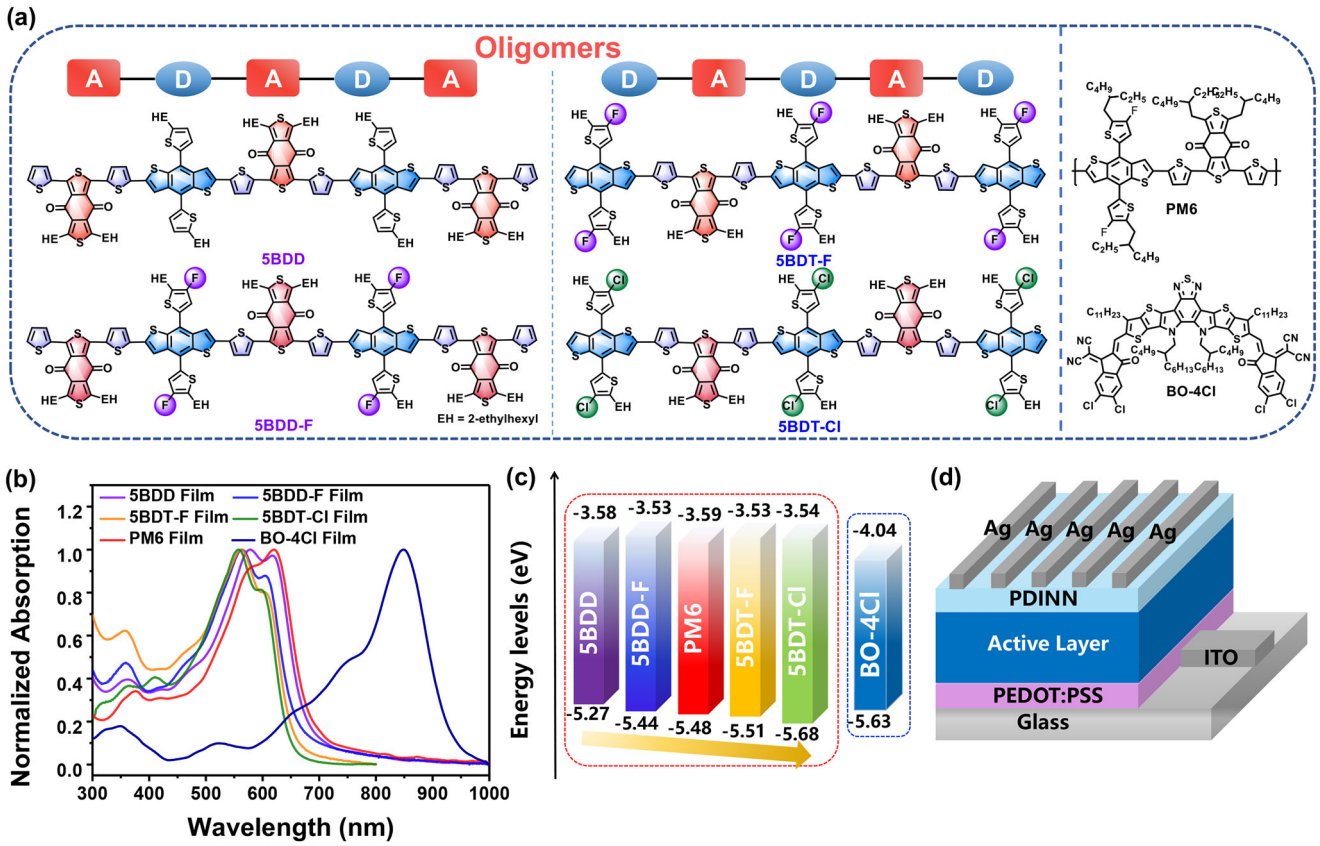

Figure 1. a) Molecular structure, b) absorption spectra of oligomers, PM6 and BO-4Cl in films, c) energy levels of 5BDD, 5BDD-F, 5BDT-F, 5BDT-Cl, PM6 and BO-4Cl in neat film, d) Schematic diagram of the conventional device structure.

−5.51 and −5.68 eV, respectively. The LUMO levels of 5BDT-F, and 5BDT-Cl were derived from the onset reduction potentials, giving values of −3.53 and −3.54 eV, respectively. These HOMO and LUMO levels are illustrated in Figure 1c and demonstrate an ordered cascade, which could potentially facilitate efficient exciton dissociation and charge transfer.[38]

2.2. Photovoltaic Properties

To evaluate the photovoltaic performance of the corresponding devices, we fabricated PM6:oligomer ternary OSCs, using the oligomer as the third component. The PM6 weight ratio was maintained at 1:1.2, with the oligomer content set at 10% by weight relative to PM6, and a halogen-free solvent (O-XY) was used. The device structure was ITO/PEDOT/Active layer/PDINN/Ag (Figure 1d), and detailed preparation steps are provided in the ESI. The current density-voltage (*J-V*) curves of these OSCs are shown in **Figure 2**a, and the corresponding device parameters are summarized in **Table 2**. The optimized binary OSCs based on PM6 achieved a PCE of 17.26%, with a V_{OC} of 0.833 V, a J_{SC} of 27.73 mA cm^{-2}, and an FF of 74.74% after TA treatment, aligning with previously reported results.[35] Notably, when 10% oligomer was introduced, the V_{OC} of the ternary devices consistently increased with TA treatment. The V_{OC} of 5BDD, 5BDD-F, 5BDT-F, and 5BDT-Cl-based ternary OSCs were 0.843, 0.844, 0.847, and 0.848 V, respectively, indicating that even a small amount of oligomer improves V_{OC}, regardless of whether its HOMO energy level is higher or lower than PM6. Encouragingly, the optimized ternary OSCs based on 5BDD, 5BDD-F, 5BDT-F, and 5BDT-Cl achieved champion PCEs of 18.27%, 18.38%, 18.39%, and 18.62%, respectively, with synergistic improvements in V_{OC}, J_{SC}, and FF. This enhancement can be attributed to optimized film morphology, efficient charge generation, and improved charge transport in the ternary devices. To further verify the V_{OC} enhancement by the oligomer, we compared the V_{OC} of the oligomer-based ternary devices with a control device without TA treatment (Figure S3 and Table S1, Supporting Information). The V_{OC} of the control device increased from 0.833 to 0.843 V, while the V_{OC} of the oligomer-based ternary devices improved significantly to 0.852, 0.855, 0.856, and 0.857 V, respectively. These results confirm that the HOMO level of the third component has minimal impact on V_{OC} improvement. Similarly, without TA treatment, the oligomer-based ternary devices achieved higher PCEs of 18.06%, 18.36%, 18.38%, and 18.43% compared to the control (17.44%), demonstrating the effectiveness of the oligomer strategy in enhancing device performance.

The external quantum efficiency (EQE) spectra of the control devices and oligomer-based ternary devices are shown in Figure 2b. The J_{SC} values calculated from the EQE spectra (Table 2) were in good agreement with those from the *J–V* curves, with an error margin of less than 5%. Compared to the

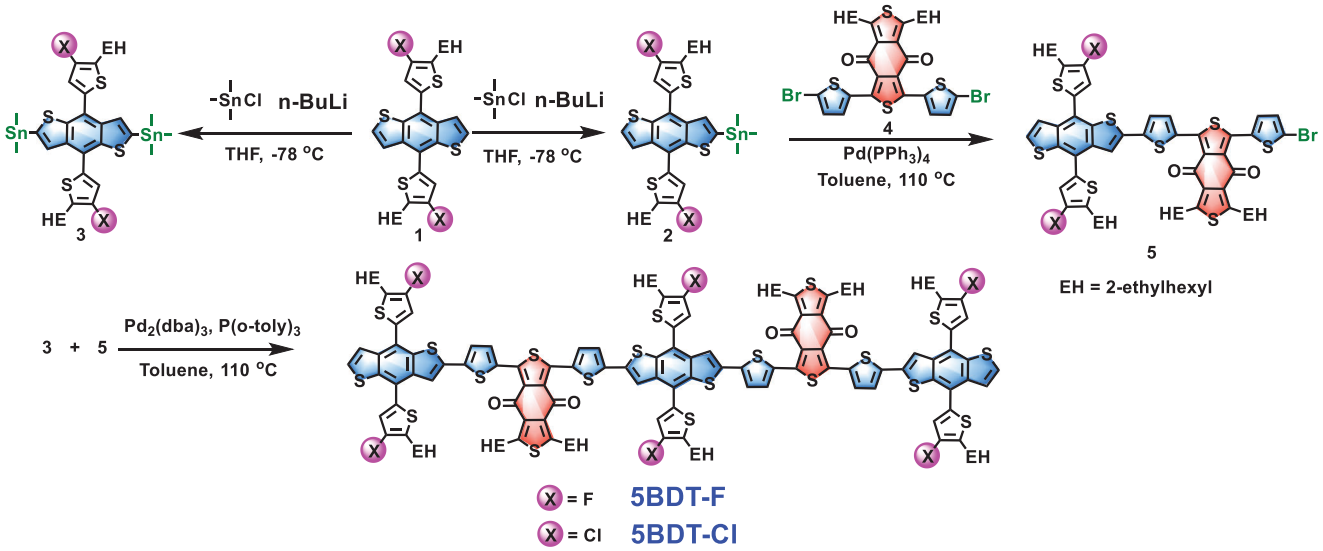

Scheme 1. Synthetic routes for 5BDT-F and 5BDT-Cl.

control device, the EQE values of the ternary blends showed significant enhancement across the 430–820 nm range. The improvement in the 430–550 nm range is attributed to the absorption contribution of the oligomers, while the enhancement in the 670–820 nm range likely arises from the optimized active layer morphology induced by the oligomers. Additionally, a negligible blue shift was observed on the right side of the EQE curve in the 850–950 nm range, which may result from suppressing small molecular acceptor aggregation due to the introduction of oligomers, leading to a corresponding blue shift in absorption. This observation aligns with the absorption characteristics of blend films containing oligomers. A more detailed discussion of this aspect will be provided in a later section. Overall, the increase in EQE effectively explains the corresponding increase in J_{SC} for the ternary devices.

2.3. Charge Separation, Transport, and Recombination

The charge dynamics of the devices were investigated to understand the reasons behind the enhanced J_{SC} and FF in oligomer-based ternary systems. The photocurrent density (J_{ph}) versus effective applied voltage (V_{eff}) curves are shown in Figure 2c. At V_{eff} >2 V, J_{ph} reaches saturation ($J_{ph} = J_{sat}$), indicating efficient exciton dissociation into electrons and holes. The exciton dissociation efficiency (η_d) is calculated as the ratio of J_{ph} to J_{sat} under short-circuit conditions. The η_d values for the ternary devices with 10% 5BDD, 10% 5BDD-F, 10% 5BDT-F, and 10% 5BDT-Cl were 98.2%, 98.3%, 98.7%, and 99.1%, respectively, all higher than that of the binary device (η_d = 98.0%). This indicates that even small amounts of oligomer can effectively enhance exciton dissociation efficiency, contributing to the improvements in both J_{SC} and FF.[39]

The charge recombination behavior of these devices was further explored by examining the relationship between J_{SC} or V_{OC} and light intensity (P_{light}). The relationship between J_{SC} and P_{light} follows the equation $J_{SC} \propto (P_{light})^{\alpha}$. [40] As shown in Figure 2d, both the control OSCs and the oligomer-based ternary OSCs exhibit high α values of 0.99, indicating minimal bimolecular recombination across all devices. Additionally, trap-assisted recombination was assessed using the relationship $V_{OC} \propto (nkT/q)lnP_{light}$, where k is Boltzmann's constant, T is the absolute temperature, and q is the elementary charge. As illustrated in Figure 2e, the slopes for the control, 10% 5BDD, 10% 5BDD-F, 10% 5BDT-F, and 10% 5BDT-Cl-based devices are 1.22 kT/q, 1.19 kT/q, 1.20 kT/q, 1.19 kT/q, and 1.16 kT/q, respectively. A smaller n value indicates weaker trap-assisted recombination. These results suggest that the oligomer-based ternary OSCs, particularly the 5BDT-Cl-based devices, exhibit the lowest levels of both bimolecular and trap-assisted recombination, contributing to the superior J_{SC} and FF performance.[41]

To further investigate carrier mobility in the control and oligomer-based ternary blend films, hole mobility (μ_h) and electron mobility (μ_e) were measured using the space-charge limited current (SCLC) method,[42] as shown in Figure S4 (Supporting Information) and summarized in Table S2 (Supporting Information). In the binary control devices, μ_h and μ_e were found to be 1.15×10^{-5} cm^2 V^{-1} s^{-2} and 1.02×10^{-4} cm^2 V^{-1} s^{-2}, respectively. Upon incorporating 10% 5BDD, 10% 5BDD-F, 10% 5BDT-F, and 10% 5BDT-Cl, μ_h increased to 1.20×10^{-4}, 1.26×10^{-4},

Table 1. Photophysical properties of 5BDD, 5BDD-F, 5BDT-F, 5BDT-Cl, and PM6.

Donor	$\lambda_{film.max}$ [nm]	$\lambda_{onset.film}$ [nm]	E_g^{opt} [eV][a)]	E_{HOMO} [eV][b)]	E_{LUMO} [eV][b)]
5BDD	577, 618	678	1.83	−5.27	−3.58
5BDD-F	563, 605	659	1.88	−5.44	−3.53
5BDT-F	557, 598	646	1.92	−5.51	−3.53
5BDT-Cl	551, 589	643	1.93	−5.68	−3.54
PM6	580, 620	684	1.81	−5.48	−3.59

[a)] Calculated from the absorption band edge of the films, $E_g^{opt} = 1240/\lambda_{onset}$; [b)] Calculated from the empirical equation: $E_{HOMO/LUMO} = -(E_{ox/red} + 4.8)$ eV.

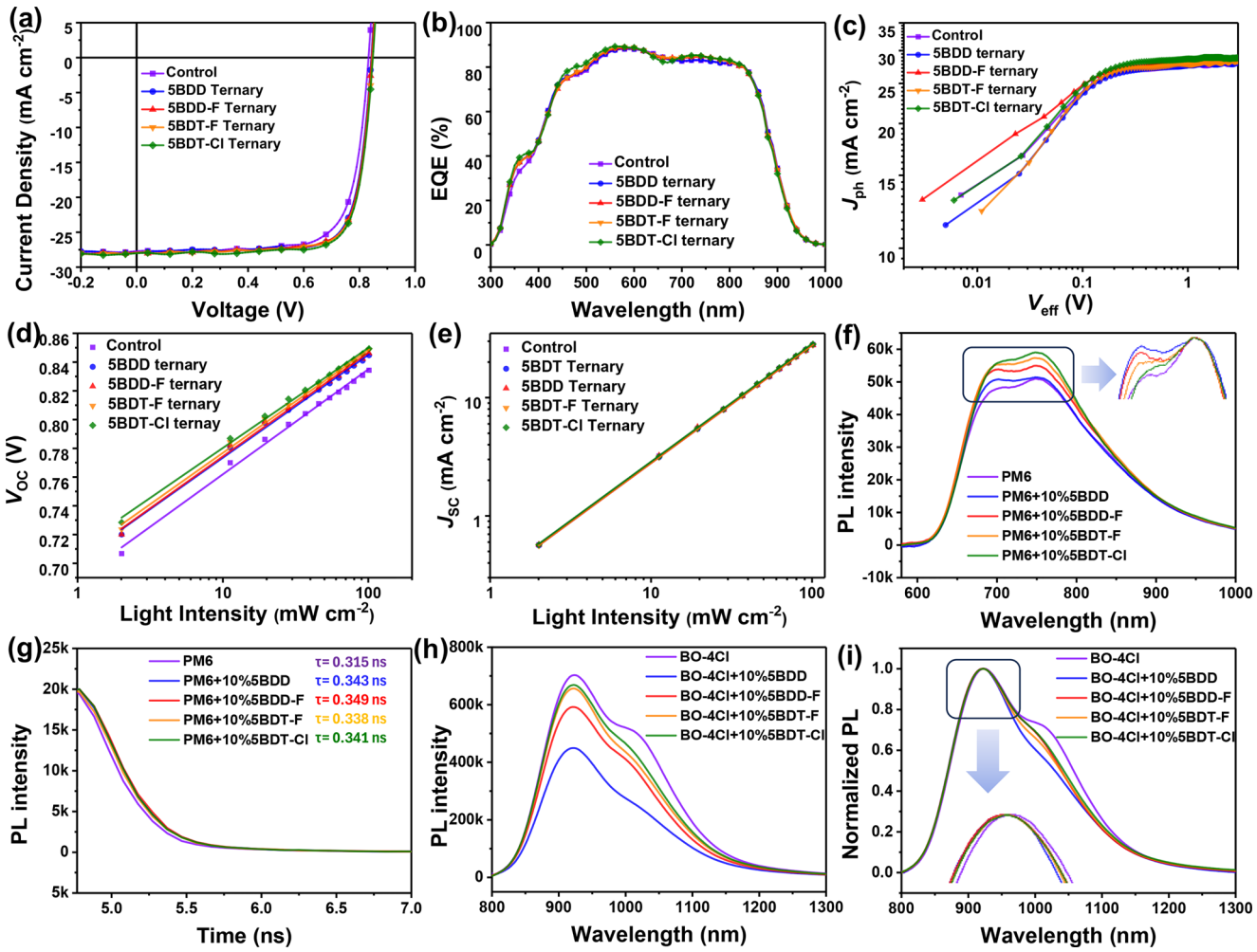

Figure 2. a) *J–V* curves and b) EQE curves of the control, 5BDD-, 5BDD-F-, 5BDT-F-, 5BDT-Cl-absed ternary devices. c) The curves of J_{ph} versus V_{eff} in the corresponding optimized solar cells. d) The dependence of P_{light} on J_{SC} of the corresponding optimized solar cells. e) The dependence of P_{light} on V_{OC} of the corresponding optimized solar cells. f) The PL spectra of PM6 neat films, and 10%oligomer-based blend film. g) The TRPL spectra of PM6 neat films, and PM6 with different 10%oligomer blend films. h) The PL spectra of BO-4Cl neat films, and BO-4Cl with different 10%oligomer-based blend films. i) The normalized PL spectra of BO-4Cl neat films, and BO-4Cl with different 10%oligomer-based blend films.

1.61×10^{-4}, and 2.01×10^{-4} cm^2 V^{-1} s^{-2}, respectively, while μe increased to 1.15×10^{-4}, 1.11×10^{-4}, 1.12×10^{-4}, and 1.17×10^{-4} cm^2 V^{-1} s^{-2}, respectively. These findings indicate that the addition of 10% oligomer significantly enhances both hole and electron mobilities, explaining the improvements in J_{SC} and FF in the optimized oligomer-based ternary devices.

To further investigate the underlying mechanism for the J_{SC} enhancement in oligomer-based ternary OSCs, we fabricated single-component devices of PM6, BO-4Cl, 5BDT-F, and 5BDT-Cl, as well as two-component devices based on PM6:oligomers and BO-4Cl:oligomers, to verify the presence of charge transfer between the oligomers and PM6 or BO-4Cl. Detailed data are provided in Table S4 (Supporting Information). The J_{SC} values of the PM6 blends were comparable to those of pure PM6 and pure oligomer-based devices, indicating an ignorable charge transfer between PM6 and the oligomers. However, the J_{SC} values of BO-4Cl devices were significantly higher than those of pure BO-4Cl and pure oligomer devices, especially in the case of BO-4Cl:5BDT-F, due to better HOMO energy level alignment. These results suggest that a charge transfer process occurs between the oligomers and BO-4Cl. The charge transfer process of BO-4Cl:oligomer favors improving charge transport in the corresponding ternary devices, which may be the reason for the higher J_{SC} of the oligomer-based ternary OSCs.

Additionally, steady-state photoluminescence (PL) and time-resolved photoluminescence (TRPL) spectroscopy were employed to investigate potential energy transfer processes between the oligomers and either PM6 or BO-4Cl, with results shown in Figure 2f–i and Figure S5 (Supporting Information). The PL spectra of the four oligomer films resemble that of PM6, positioned within the 600–1000 nm range, but their emission intensity is weaker than that of PM6. Notably, the PL spectra partially overlap with the absorption regions of both PM6 and BO-4Cl, suggesting the potential for energy transfer between these components.[43] As illustrated in Figure 2f, the emission intensity of the PM6:10% oligomer blend films are more than 10% higher than that of the

Table 2. The photovoltaic parameters of the binary and ternary devices.

Active layer	Treatment	V_{OC} [V]	J_{SC}[a] [mA cm^{-2}]	J_{SC}^{EQE} [mA cm^{-2}]	FF [%]	PCE_{max}[b] [%]
Control[c]	TA	0.833	27.73	26.46	74.74	17.26 (17.12 ± 0.17)
5BDD ternary[c]	TA	0.843	27.90	26.53	77.69	18.27 (18.18 ± 0.10)
5BDD-F ternary[c]	TA	0.844	27.92	26.61	77.98	18.38 (18.24 ± 0.15)
5BDD-F ternary[c]	TA	0.847	27.95	26.67	77.65	18.37 (18.22 ± 0.14)
5BDD-Cl ternary[c]	TA	0.848	28.02	26.72	78.34	18.62 (18.52 ± 0.08)

[a] J_{SC} measured from devices; [b] PCE obtained from 15 devices, with 0.5% DIO additive; [c] PM6:Oligomer:BO-4Cl = 10:1:12 mg mL^{-1}, the concentration of PM6 is 10 mg mL^{-1}.

pure PM6 films, indicating the presence of energy transfer from the oligomers to PM6. The normalized PL spectra (Figure 2f) show ignorable shifts in the PL peaks of the PM6 blends compared to pure PM6, suggesting that the oligomers have little impact on the aggregation state of PM6. In contrast, when investigating the energy transfer between the oligomers and BO-4Cl (Figure 2h), the PL intensity of BO-4Cl was reduced upon the introduction of oligomers, implying the presence of charge transfer from BO-4Cl to the oligomers.[44] Interestingly, the decrease in PL intensity correlates with the HOMO energy levels of the oligomers, further supporting the existence of charge transfer between BO-4Cl and the oligomers. Additionally, the normalized PL spectra show a slight blue shift in the PL peaks of the BO-4Cl blend films compared to pure BO-4Cl, and the characteristic BO-4Cl PL peak near 1030 nm nearly disappears in the blends, indicating that the oligomers inhibit BO-4Cl aggregation, consistent with UV absorption results.

To evaluate the charge transfer situation in control and ternary devices, the PM6 neat film, control, and ternary blend films were excited with 500 nm of light, and an intense emission peak was observed in the PM6 neat film (600–800 nm). The emission of the PM6 is almost completely quenched in control, 5BDD, 5BDD-F, 5BDD-F, and 5BDD-Cl-based ternary blend films with high quenching efficiencies of 99%. The results show that both blend films exhibit efficient charge transfer from donor to acceptor.[45] Interestingly, the blend films all exhibited distinct emission peaks around 930 nm, which aligned with the emission peaks of the pure acceptor BO-4Cl, suggesting that the residual energy of the excitation light source excites the ground state of BO-4Cl (Figure S5, Supporting Information). Notably, the emission intensity of the oligomer-based blend films was significantly higher than that of the control binary blends, and this enhancement increased as the HOMO energy level of the oligomer decreased. Furthermore, the emission peaks of the oligomer-based blends were blue-shifted compared to the control, indicating that the introduction of oligomers inhibits the aggregation of the acceptor, consistent with earlier observations. In addition, the significantly enhanced emission intensity likely contributes to the improvement in the EQE_{EL}, which could explain the higher V_{OC} observed in the oligomer-based ternary devices. Furthermore, the BO-4Cl neat film, control, and ternary blend films were excited with 800 nm light, resulting in an intense emission peak in the BO-4Cl neat film (800–1300 nm range). As shown in Figure S5d (Supporting Information), the emission from BO-4Cl was almost entirely quenched in both the control and ternary blend films, with high quenching efficiencies of 98.8%, 98.4%, 98.2%, 98.2%, and 98.3%, respectively. These results demonstrate that both the control and ternary blend films enable efficient charge transfer from the acceptor to the donor.[46] Additionally, the slightly higher PL intensities observed in the ternary devices compared to the control may contribute to the increased V_{OC}. Additionally, time-resolved photoluminescence (TRPL) measurements were conducted to investigate both PM6 neat films and PM6 films blended with 10%5BDD, 10%5BDD-F, 10%5BDT-F, and 10%5BDT-Cl (Figure 2h). The lifetime of the PM6 neat film was 0.315 ns, while the lifetimes of the PM6 blend films increased to 0.343, 0.349, 0.338, and 0.341 ns, respectively. This increase in lifetime indicates efficient energy transfer from the oligomers to PM6, which provides a plausible explanation for the enhanced J_{SC} observed in the oligomer-based ternary devices.[47]

To further explore the dynamics of photo-induced hole transfer and polaron recombination in these blend films, femtosecond transient absorption spectroscopy (fs-TAS) was employed. An 800 nm pump laser beam selectively excited the BO-4Cl, allowing for a comparative analysis of the time-dependent spectral evolution between the control and oligomer-based blend films (**Figure 3**). As the delay time progressed, the ground state bleaching (GSB) signal of the BO-4Cl singlet exciton was observed in the 700–880 nm range. This signal initially increased, corresponding to the absorption of photon energy by ground-state electrons to form excitons, and then decayed as these excitons either dissociated into free charges or returned to the ground state. Additionally, the GSB signal of PM6 appeared in the 550–680 nm range in all blend films, which was in excellent accordance with the absorption characteristics of PM6 (Figure 1b). The observed decay in the singlet exciton GSB aligned with polaron photo-bleaching in the 880–950 nm range, suggesting efficient hole transfer between the acceptor and donor. The decay lifetimes of singlet excitons (probe at 827 nm) in the control, 5BDD, 5BDD-F, 5BDT-F, and 5BDT-Cl-based ternary blends were 0.589, 0.606, 0.669, 0.662, and 0.665 ps, respectively. Likewise, polaron decay lifetimes (probe at 943 nm) were 0.734, 0.767, 0.780, 0.764, and 0.817 ps, respectively. The extended lifetimes of singlet excitons and polarons in the oligomer-based ternary blends may be due to the reduced aggregation of BO-4Cl. Notably, this slower decay process does not necessarily hinder charge generation; it can actually optimize the nanomorphology, mobility, and interfacial energetics.[48] In fact, slower processes may even support and enhance charge

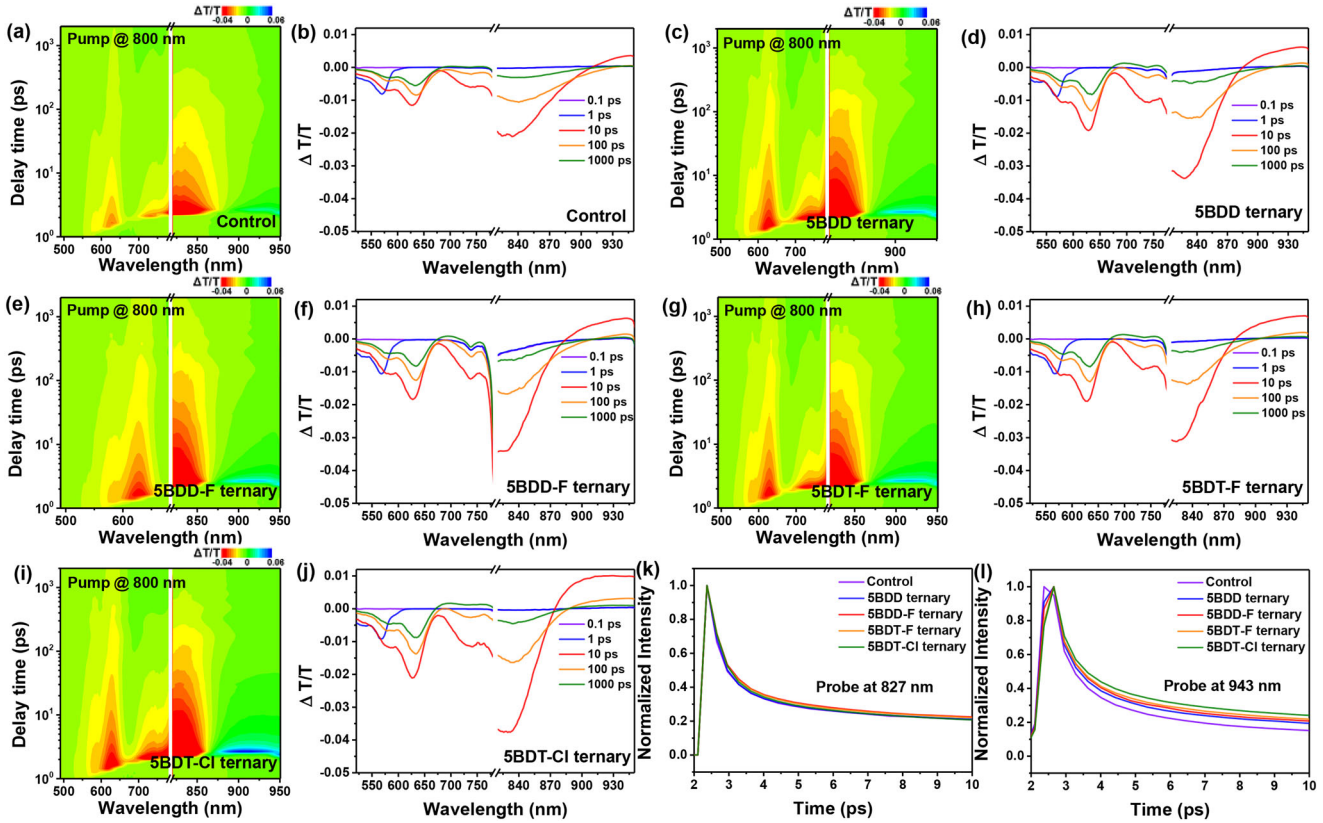

Figure 3. a,c,e,g,i) 2D color plot of fs-TA spectra of control, oligomer-based ternary blend at indicated delay times under 800 nm excitation with a fluence below 10 μJ cm^{-2}. b,d,f,h,j) The fs-TA spectra of control, oligomer-based ternary blend at indicated delay times. g) Lifetime of single exciton with the corresponding blend films. h) polaron generation dynamics with the corresponding blend films.

generation, contributing to the high efficiency of these ternary blends despite the delayed decay.[49]

Grazing-incidence wide-angle X-ray scattering (GIWAXS) was conducted to assess the molecular aggregation and crystallinity of the blend films. **Figure** 4a–e presents the GIWAXS 2D patterns, and the line-cut profiles along the out-of-plane (OOP) and in-plane (IP) directions are shown in Figure 4f,g. The (100) diffraction peaks in the IP direction of both the control and oligomer-based ternary blend films were located consistently at 0.299 $Å^{-1}$ (d = 20.93 Å). Meanwhile, the OOP (100) diffraction peaks for the control and oligomer-based films appeared at 0.301 $Å^{-1}$ (d = 20.86 Å), 0.294 $Å^{-1}$ (d = 21.36 Å), 0.299 $Å^{-1}$ (d = 21.00 Å), 0.300 $Å^{-1}$ (d = 20.93 Å), and 0.295 $Å^{-1}$ (d = 21.28 Å), respectively. For the (010) diffraction peaks in the OOP direction, all blend films showed similar values at 1.75 $Å^{-1}$ (d = 3.58 Å), with corresponding coherence lengths (CCLs) of 16.67, 16.62, 16.62, 16.97, and 17.23 Å, respectively. However, both (100) and (010) peak intensities of oligomer-based ternary blend films are slightly weaker than those of control blend films. Based on the above results, it is evident that the introduction of 10% oligomer has no obvious effect on the host molecular aggregation and crystallization, but slightly inhibits the excessive aggregation of BO-4Cl acceptor (consistent with the slightly blue-shifted absorption of the oligomer-based ternary blend films), fine-tuning and optimizing the morphology of the active layer.[50] The suppressed excessive aggregation of BO-4Cl improves the luminous efficiency and facilitates inhibition of the charge recombination, this is the reason for the higher V_{OC} and FF of oligomer-based three components.

The morphological changes in the blend films induced by the oligomers were further analyzed using atomic force microscopy (AFM). As illustrated in Figure 4a–e,m and Figure S6 (Supporting Information), the root-mean-square (RMS) roughness values of the oligomer-based ternary blend films were marginally lower than that of the control blend film (1.29, 1.27, 1.26, and 1.26 nm compared to 1.30 nm), suggesting improved miscibility of the oligomers with PM6 and BO-4Cl. This enhanced miscibility appears to moderately suppress aggregation within the active layer materials, consistent with the UV–vis and GIWAXS results.[51] Additionally, the ternary blends incorporating oligomers displayed more pronounced fiber-like structures, indicating that the oligomers effectively fine-tune the morphology of the blend films.

The compatibility between active layer components plays a crucial role in influencing phase separation. Here, contact angle (CA) measurements were used to evaluate the surface energy of each component in both water and ethylene glycol (EG). As shown in Figure 4j and Figure S7 (Supporting Information), the water contact angles of PM6, BO-4Cl, 5BDD, 5BDD-F, 5BDT-F, and 5BDT-Cl neat films were 103.147°, 98.292°, 103.672°, 103.838°, 103.692°, and 103.711°, respectively. Besides, the EG contact angles for these films were recorded as 76.219°, 70.613°, 75.777°, 75.799°, 75.756°, and 75.431°, respectively. Using Wu's

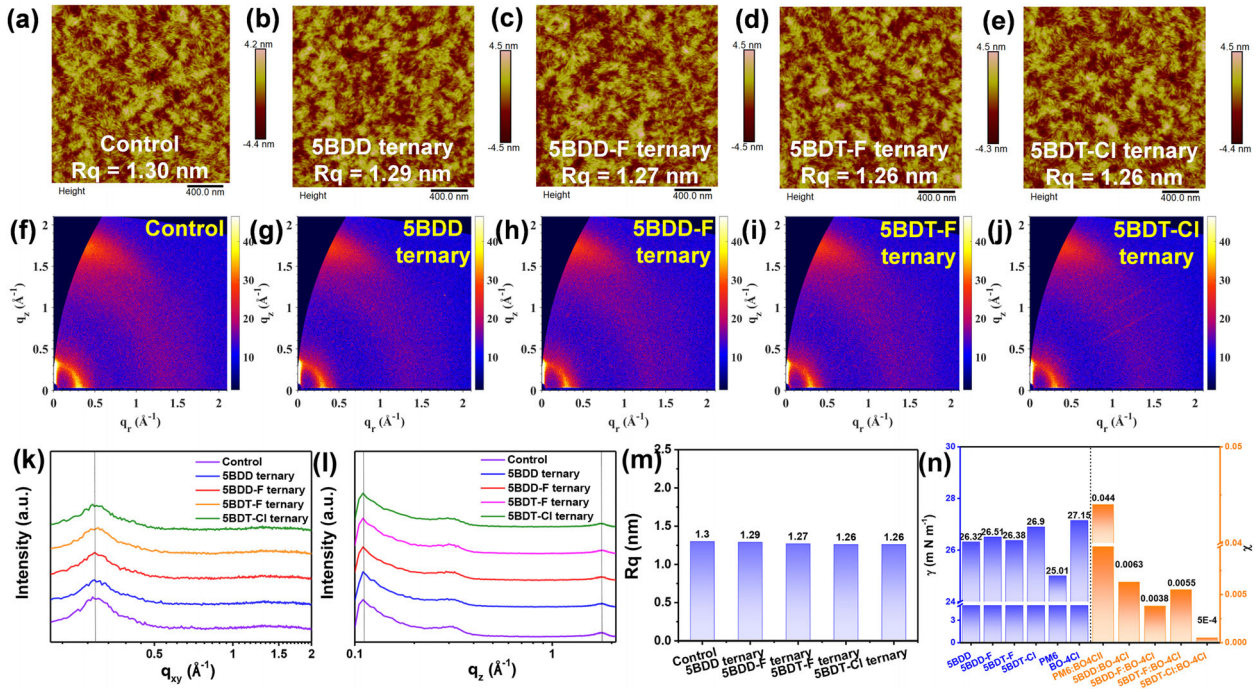

Figure 4. a–e) AFM high images of control, oligomer-based ternary blend films. 2D GIWAXS patterns of f) control, g) 5BDD-based ternary film, h) 5BDD-F-based ternary film, i) 5BDT-F-based ternary film, and j) 5BDT-Cl-based ternary film. The 1D line cuts along k) in-plane and l) out-of-plane of the corresponding films. m) The RMS value of corresponding blend films. n) The surface energy values and χ values of corresponding neat films and blend films.

model,[52] we calculated the dispersion force (γ^d), polar force (γ^p), and surface tension (γ) of these films, with results summarized in Table S3 (Supporting Information). The surface tension values for PM6, BO-4Cl, 5BDD, 5BDD-F, 5BDT-F, and 5BDT-Cl films were found to be 25.005, 27.147, 26.323, 26.508, 26.381, and 26.904 mN m^{-1}, respectively. Additionally, the Flory-Huggins interaction parameter (χ) was employed to evaluate the compatibility between these components.[53] Calculated as $\chi_{A-B} = K(\sqrt{\gamma_A} - \sqrt{\gamma_B})^2$, where γ_A and γ_B denote the surface tensions of A and B, respectively. The χ values were 0.044, 0.0063, 0.0038, 0.0055, and 0.0005 K for $\chi_{PM6-BO-4Cl}$, $\chi_{5BDD-BO-4Cl}$, $\chi_{5BDD-F-BO-4Cl}$, $\chi_{5BDT-F-BO-4Cl}$ and $\chi_{5BDT-Cl-BO-4Cl}$, respectively, as shown in Table S3 (Supporting Information). These values suggest superior miscibility between the oligomers and BO-4Cl. Consequently, the introduction of these oligomers might impact the aggregation state of BO-4Cl, effectively optimizing the morphology of the active layer.

2.4. Energy Loss Analysis

The enhanced V_{OC} is a key factor in achieving higher efficiency in oligomer-based ternary OSCs. To better understand the mechanism behind the significant increase in V_{OC} with the introduction of oligomers with varying HOMO levels as the third component, we investigated the detailed energy losses (E_{loss}) in both control and oligomer-based ternary devices. In OSCs, the E_{loss} can be divided into three components.[54] ΔE_1 represents the radiative recombination loss resulting from the absorption of photons above the bandgap, which is inherent to all types of solar cells. ΔE_2 accounts for additional radiative recombination from photons absorbed below the bandgap. ΔE_3 denotes non-radiative recombination loss, which can be evaluated using the formula $-kT\ln EQE_{EL}$, where EQE_{EL} is the external electroluminescence quantum efficiency of the solar cells. Notably, an increase in EQE_{EL} correlates with a reduction in ΔE_3, leading to a higher V_{OC}. This implies that an ideal photovoltaic device, devoid of non-radiative recombination, would function as a perfect light-emitting diode (LED).[55] The values of E_{gap} of all devices were derived from the derivative of EQE_{PV} spectral edge (dEQE/dE), ΔE_3 was calculated by EQE_{EL}, as shown in **Table 3** and **Figures 5** and S8 (Supporting Information). The E_{gap}s values of the control binary device and the oligomer-based ternary devices are 1.408, 1.403, 1.402, 1.401, and 1.400 eV, respectively. All devices display similar ΔE_1 values (0.262 eV) and minimal ΔE_2 values (ranging from 0.076 to 0.065 eV). As illustrated in Figure 5, the addition of oligomers reduces ΔE_3 values due to the enhanced EQE_{EL} of the oligomer-based devices. The EQE_{EL} values of control binary devices, oligomer-based ternary devices are 1.05×10^{-4}, 1.62×10^{-4}, 1.67×10^{-4}, 1.66×10^{-4}, and 1.70×10^{-4}, respectively, and the corresponding ΔE_3 are calculated as 0.237, 0.226, 0.225, 0.225, and 0.225 eV, respectively. Finally, the V_{OC} loss of these devices was 0.575, 0.560, 0.558, 0.554, and 0.552 eV, respectively, aligning with the V_{OC} improvement in the oligomer-based ternary OSCs. Moreover, the energetic disorder in OSCs, evaluated through the Urbach energy (Eu), provides insight into the trap states. The Urbach energy, determined by fitting the FTPS-EQE absorption edge in the lower energy region, follows the equation: $\alpha(E) = \alpha_0 e^{\frac{E-E_g}{E_U}}$.[4] The low values indicate reduced energetic

Table 3. Summary of energy loss parameters of binary and ternary devices based on PM6:oligomer:BO-4Cl system measured and calculated from FTPS-EQE and EL.

Device	E_g [a)] [eV]	V_{OC} [V]	ΔE [eV]	V_{OC}^{SQ} [V]	V_{OC}^{rad} [V]	EQE_{EL} [%]	ΔE_1 [eV]	ΔE_2 [eV]	ΔE_3 [eV]
Control	1.391	0.833	0.558	1.131	1.070	1.05×10^{-2}	0.260	0.061	0.237
10%5BDD ternary	1.392	0.843	0.549	1.132	1.069	1.62×10^{-2}	0.260	0.063	0.226
10%5BDD-F ternary	1.393	0.844	0.549	1.133	1.069	1.67×10^{-2}	0.260	0.064	0.225
10%5BDT-F ternary	1.394	0.847	0.547	1.133	1.072	1.66×10^{-2}	0.261	0.061	0.225
10%5BDT-Cl ternary	1.396	0.848	0.548	1.135	1.073	1.70×10^{-2}	0.261	0.062	0.225

[a)] E_g was obtained from the derivatives of the EQE_{PV} spectra.

disorder and fewer trap states, and the Eu values of the control and oligomer-based devices are 28.1, 27.2, 27.0, 27.0, and 26.9 meV, showing that the oligomers suppress trap states. This suppression contributes to lower radiative and non-radiative recombination losses. Thus, the reduced energy losses are attributed more to decreased energetic disorder and trap states enabled by optimized morphology than to the energy level-dominant V_{OC} increment mechanisms commonly cited in previous ternary studies.[56]

2.5. Universality

To assess the broader applicability of the oligomer ternary strategy, we modified the processing solvent from O-XY to CB in

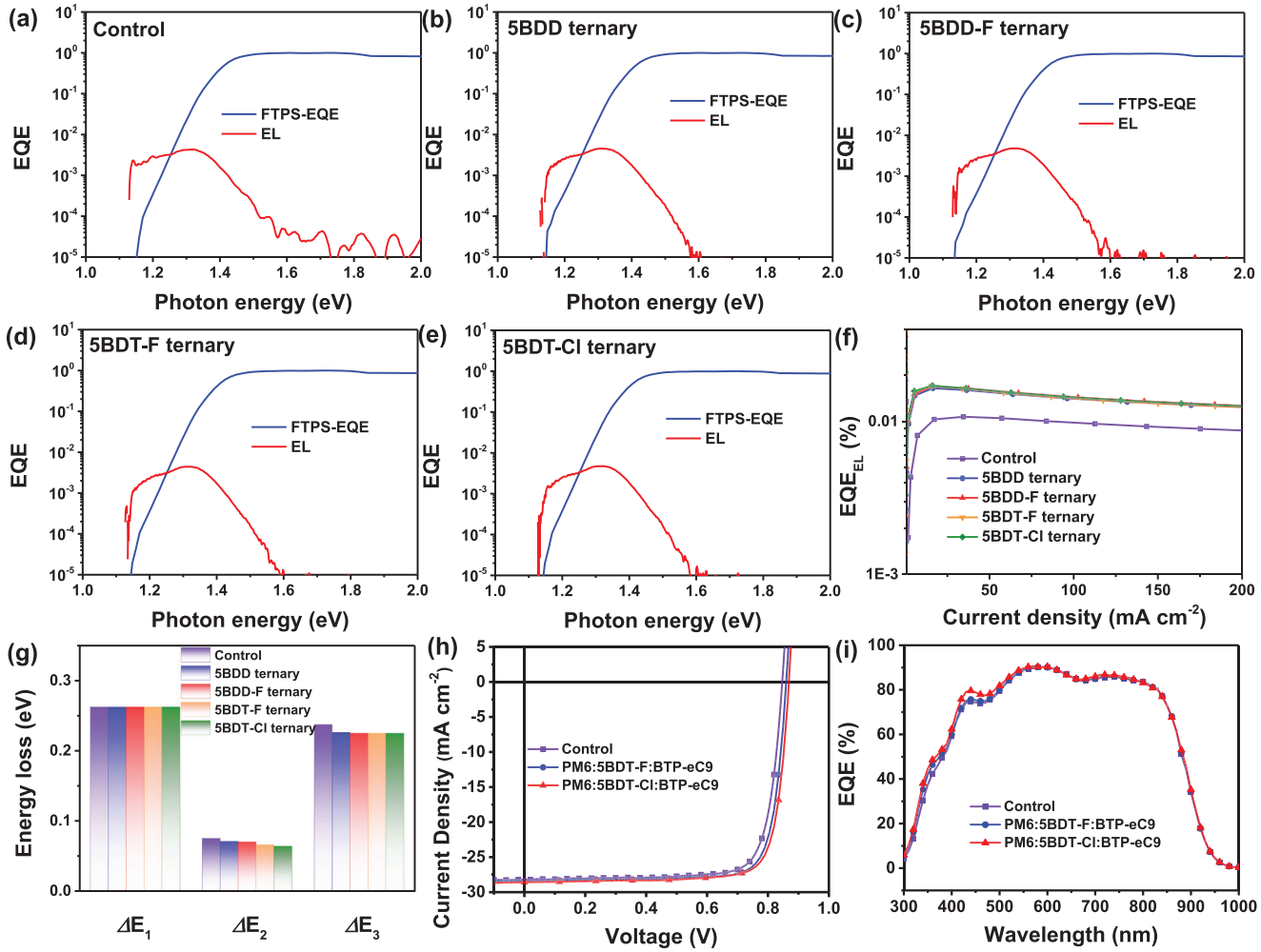

Figure 5. a–e) The normalized FTPS-EQE and EL spectra of different OSCs. f) The EQE_{EL} spectra of different OSCs. g) ΔE_1, ΔE_2, and ΔE_3 values of different OSCs. h) The *J*—*V* cures of different OSCs. i) The EQE cures of different OSCs.

Table 4. The photovoltaic parameters of the binary and ternary devices.

Active layer	Treatment	V_{OC} [V]	J_{SC}[a] [mA cm^{-2}]	J_{SC}^{EQE} [mA cm^{-2}]	FF [%]	PCE_{max}[b] [%]
Control[c]	TA	0.847	28.2	27.1	79.5	19.0 (18.7 ± 0.1)
5BDT-F ternary[c]	TA	0.860	28.4	27.2	80.9	19.8 (19.5 ± 0.1)
5BDT-Cl ternary[c]	TA	0.869	28.6	27.5	80.7	20.1 (19.7 ± 0.2)
5BDT-Cl ternary[d]	TA	0.858	28.53	–	80.71	19.76 (Certified)

[a] J_{SC} measured from devices; [b] PCE obtained from 15 devices, with DIB as additive (10 mg mL^{-1}); [c] PM6:Oligomer:BTP-eC9 = 10:1:12 mg mL^{-1}, the concentration of PM6 is 10 mg mL^{-1}; [d] The certified PCE from Chengdu Institute of Product Quality Inspection Co., Ltd and National Photovoltaic Product Quality Inspection & Testing Center, China.

a classical system of PM6:BTP-eC9 using DIO as an additive. The *J-V* and EQE curves for the PM6:oligomer devices using CB are shown in Figure S9 (Supporting Information), respectively, with key parameters listed in Table S4 (Supporting Information). Compared to the PM6 binary control devices, all oligomer-based ternary devices displayed a notable V_{OC} enhancement, increasing from 0.850 V in the control to 0.856, 0.857, 0.858, and 0.859 V, respectively. This trend aligns with that observed in oligomer-based devices processed with O-XY, although the V_{OC} increase is slightly reduced with CB processing due to CB's higher solubility, which lessens the ACQ suppression effect. Additionally, the FF rose from approximately 78% in the control devices to over 79% in the oligomer-based ternary devices, with overall performance improving from 18.26% in the control to 18.64%, 18.80%, 19.15%, and 19.10%, respectively. These findings validate the effectiveness of the oligomer ternary strategy across different processing conditions.

Furthermore, we investigated the universality of this oligomer ternary strategy in another mainstream OSCs blend, PM6:BTP-eC9. Here, PM6:5BDT-F:BTP-eC9 and PM6:5BDT-Cl:BTP-eC9-based devices were fabricated using CB as a processing solvent, and DIB was used as the additive instead of DIO.[57] The *J–V* and EQE curves for PM6:oligomer:BTP-eC9-based devices are presented in Figure 5, and the relevant data are summarized in **Table 4**. The PM6:5BDT-F:BTP-eC9-based and PM6:5BDT-Cl:BTP-eC9-based ternary devices obtained excellent PCEs of 19.8% with a V_{OC} of 0.865 V, a J_{SC} of 28.4 mA cm^{-2}, a FF of 80.9%, and 20.1% (certified 19.76%, ESI) with a V_{OC} of 0.869 V, J_{SC} of 28.6 mA cm^{-2}, a FF of 80.7%, respectively, which are obviously higher than the PM6:BTP-eC9-based devices of 19.0%. The performance improvement of these devices contributes to the optimized effect of the DIB additive for the morphology of the active layer, exhibiting the superiority of the DIB additive. Meanwhile, the V_{OC} of 5BDT-F-based and 5BDT-Cl-based ternary devices still achieves improvement compared to control devices, indicating the universality of the oligomer ternary strategy. It is important to note that these oligomer-based OSCs represent state-of-the-art OSCs.

3. Conclusion

In this study, via modular molecular design, we introduced a series of oligomeric donors with systematically tuned energy levels –5BDD, 5BDD-F, 5BDT-F, and 5BDT-Cl– as third components in ternary OSCs, demonstrating that the HOMO levels of these oligomers exert an ignorable effect on V_{OC}. Instead, the V_{OC} enhancement observed across all ternary devices was attributed to the excellent compatibility of these oligomers with non-fullerene acceptors, which mitigated acceptor over-aggregation and reduced the ACQ effect. This interaction improved the EQE_{EL} and reduced non-radiative recombination loss. Additionally, these oligomers fine-tuning and optimized the blend film morphology, leading to a higher FF and improved device performance. Notably, ternary OSCs based on 5BDT-F and 5BDT-Cl achieved excellent PCEs of 19.8% and 20.1% (certified 19.76%), with V_{OC} values of 0.867 and 0.869 V, and FFs of 80.9% and 80.7%, respectively. These findings reveal the critical role of compatibility between the third component and the acceptor in boosting V_{OC}, providing a valuable framework for designing high-efficiency ternary OSCs with optimized V_{OC} values.

Supporting Information

Supporting Information is available from the Wiley Online Library or from the author.

Acknowledgements

This work was supported by the Research Grants Council of Hong Kong (Project Nos. C7018-20G, C4005-22Y), RGC Senior Research Fellowship Scheme (SRFS2223-5S01), the Hong Kong Polytechnic University (Sir Sze-yuen Chung Endowed Professorship Fund (8-8480), RISE (Q-CDBK), PRI (Q-CD7X)). Thanks to the financial support from the National Natural Science Foundation of China (22275024, 51673031), the "Seed Plan" Project of China Petroleum and Chemical Corporation (223298), Changzhou Social Development Project (CZ20220027), Jiangsu Provincial Talents Project of High-Level Innovation and Entrepreneurship.

Conflict of Interest

The authors declare no conflict of interest.

Author Contributions

W.Z., G.L., and H.X. conceived the concept and designed the experiments. H.X. conducted all experimental work and contributed to the manuscript writing. J.F. assisted with device fabrication. C.Y. supported PL and TRPL measurements. D.L. and R.M. carried out TAS measurements. H.L. and X.L. performed GIWAXS measurements. Y.L. provided expertise and data for EQE_{EL} and FTPS-EQE measurements. W.Z. and G.L. supervised the project and contributed to the manuscript revision.

Data Availability Statement

The data that support the findings of this study are available from the corresponding author upon reasonable request.

Keywords

compatibility, energy loss, green solvents, oligomer donors, ternary organic solar cells

Received: January 20, 2025
Revised: March 19, 2025
Published online: June 27, 2025

[1] G. Yu, J. Gao, J. C. Hummelen, F. Wudl, A. J. Heeger, *Science* **1995**, *270*, 1789.
[2] G. Li, R. Zhu, Y. Yang, *Nat. Photonics* **2012**, *6*, 153.
[3] L. Dou, Y. Liu, Z. Hong, G. Li, Y. Yang, *Chem. Rev.* **2015**, *115*, 12633.
[4] J. Hou, O. Inganäs, R. H. Friend, F. Gao, *Nat. Mater.* **2018**, *17*, 119.
[5] H. Yin, C. Yan, H. Hu, J. K. W. Ho, X. Zhan, G. Li, S. K. So, *Mater. Sci. Eng.: R: Rep.* **2020**, *140*, 100542.
[6] M. Günther, N. Kazerouni, D. Blätte, J. D. Perea, B. C. Thompson, T. Ameri, *Nat. Rev. Mater.* **2023**, *8*, 456.
[7] P. Ding, D. Yang, S. Yang, Z. Ge, *Chem. Soc. Rev.* **2024**, *53*, 2350.
[8] M. Wu, B. Ma, S. Li, J. Han, W. Zhao, *Adv. Funct. Mater.* **2023**, *33*, 2305445.
[9] X. Yu, P. Ding, D. Yang, P. Yan, H. Wang, S. Yang, J. Wu, Z. Wang, H. Sun, Z. Chen, *Angew. Chem.* **2024**, *136*, 202401518.
[10] Y. Cui, P. Zhu, H. Hu, X. Xia, X. Lu, S. Yu, H. Tempeld, R. A. Eichel, X. Liao, Y. Chen, *Angew. Chem., Int. Ed.* **2023**, *62*, 202304931.
[11] T. Dai, A. Tang, Y. Meng, C. Dong, P. Cong, J. Lu, J. Du, Y. Zhong, E. Zhou, *Angew. Chem., Int. Ed.* **2024**, *63*, 202403051.
[12] Z. Wang, X. Wang, L. Tu, H. Wang, M. Du, T. Dai, Q. Guo, Y. Shi, E. Zhou, *Angew. Chem.* **2024**, *136*, 202319755.
[13] W. Song, Q. Ye, S. Yang, L. Xie, Y. Meng, Z. Chen, Q. Gu, D. Yang, J. Shi, Z. Ge, *Angew. Chem.* **2023**, *135*, 202310034.
[14] Q. Fan, R. Ma, J. Yang, J. Gao, H. Bai, W. Su, Z. Liang, Y. Wu, L. Tang, Y. Li, *Angew. Chem.* **2023**, *135*, 202308307.
[15] L. Lu, M. A. Kelly, W. You, L. Yu, *Nat. Photonics* **2015**, *9*, 491.
[16] P. Bi, X. Hao, *Sol. RRL* **2019**, *3*, 1800263.
[17] R. Yu, H. Yao, J. Hou, *Adv. Energy Mater.* **2018**, *8*, 1702814.
[18] Y. Zhang, G. Li, *Acc. Mater. Res.* **2020**, *1*, 158.
[19] N. Gasparini, A. Salleo, I. McCulloch, D. Baran, *Nat. Rev. Mater.* **2019**, *4*, 229.
[20] M. Jiang, H.-F. Zhi, B. Zhang, C. Yang, A. Mahmood, M. Zhang, H. Y. Woo, F. Zhang, J.-L. Wang, Q. An, *ACS Energy Lett.* **2023**, *8*, 1058.
[21] H. Xia, M. Zhang, H. Wang, Y. Sun, Z. Li, R. Ma, H. Liu, T. A. Dela Peña, H. T. Chandran, M. Li, *Adv. Funct. Mater.* **2024**, *34*, 2411058.
[22] J. Guo, X. Xia, B. Qiu, J. Zhang, S. Qin, X. Li, W. Lai, X. Lu, L. Meng, Z. Zhang, *Adv. Mater.* **2023**, *35*, 2211296.
[23] Q. Fan, R. Ma, Z. Bi, X. Liao, B. Wu, S. Zhang, W. Su, J. Fang, C. Zhao, C. Yan, *Adv. Funct. Mater.* **2023**, *33*, 2211385.
[24] H. Lu, W. Liu, G. Ran, J. Li, D. Li, Y. Liu, X. Xu, W. Zhang, Z. Bo, *Adv. Mater.* **2024**, *36*, 2307292.
[25] W. Tang, Z. Ding, Y. Su, Q. Weng, Y. Zhang, R. Li, W. Huang, Z. Wang, Y. Wu, Y. Han, *Adv. Funct. Mater.* **2024**, *34*, 2312289.
[26] N. Y. Doumon, L. Yang, F. Rosei, *Nano Energy* **2022**, *94*, 106915.
[27] X. Xu, Y. Li, Q. Peng, *Adv. Mater.* **2022**, *34*, 2107476.
[28] K. Zhou, K. Xian, R. Ma, J. Liu, M. Gao, S. Li, T. Liu, Y. Chen, Y. Geng, L. Ye, *Energy Environ. Sci.* **2023**, *16*, 5052.
[29] Y. Cai, C. Xie, Q. Li, C. Liu, J. Gao, M. H. Jee, J. Qiao, Y. Li, J. Song, X. Hao, *Adv. Mater.* **2023**, *35*, 2208165.
[30] Y. Yue, B. Zheng, J. Ni, W. Yang, L. Huo, J. Wang, L. Jiang, *Adv. Sci.* **2022**, *9*, 2204030.
[31] S. Liu, J. Wang, S. Wen, F. Bi, Q. Zhu, C. Yang, C. Yang, J. Chu, X. Bao, *Adv. Mater.* **2024**, *36*, 2312959.
[32] Q. An, J. Wang, X. Ma, J. Gao, Z. Hu, B. Liu, H. Sun, X. Guo, X. Zhang, F. Zhang, *Energy Environ. Sci.* **2020**, *13*, 5039.
[33] W. Zou, C. Han, X. Zhang, J. Qiao, J. Yu, H. Xu, H. Gao, Y. Sun, Y. Kan, X. Hao, *Adv. Energy Mater.* **2023**, *13*, 2300784.
[34] H. Xia, Y. Zhang, W. Deng, K. Liu, X. Xia, C. J. Su, U. S. Jeng, M. Zhang, J. Huang, J. Huang, *Adv. Mater.* **2022**, *34*, 2107659.
[35] H. Xia, Y. Zhang, K. Liu, W. Deng, M. Zhu, H. Tan, P. W. Fong, H. Liu, X. Xia, M. Zhang, *Energy Environ. Sci.* **2023**, *16*, 6078.
[36] H. Xia, X. Xu, C. Qian, J. Guo, J. Zhao, K. Zhang, H. Tan, Q. Peng, W. Zhu, *ACS Appl. Energy Mater.* **2022**, *5*, 3146.
[37] J. Fu, P. W. Fong, H. Liu, C.-S. Huang, X. Lu, S. Lu, M. Abdelsamie, T. Kodalle, C. M. Sutter-Fella, Y. Yang, *Nat. Commun.* **2023**, *14*, 1760.
[38] Y. Zhang, W. Deng, C. E. Petoukhoff, X. Xia, Y. Lang, H. Xia, H. Tang, H. T. Chandran, S. Mahadevan, K. Liu, *Joule* **2024**, *8*, 509.
[39] P. W. Blom, V. D. Mihailetchi, L. J. A. Koster, D. E. Markov, *Adv. Mater.* **2007**, *19*, 1551.
[40] L. Nian, K. Gao, Y. Jiang, Q. Rong, X. Hu, D. Yuan, F. Liu, X. Peng, T. P. Russell, G. Zhou, *Adv. Mater.* **2017**, *29*, 1700616.
[41] L. J. A. Koster, V. D. Mihailetchi, R. Ramaker, P. W. Blom, *Appl. Phys. Lett.* **2005**, *86*, 123509.
[42] N. Yi, Q. Ai, W. Zhou, L. Huang, L. Zhang, Z. Xing, X. Li, J. Zeng, Y. Chen, *Chem. Mater.* **2019**, *31*, 10211.
[43] K. Zhang, Z. Jiang, J. Qiao, P. Lu, C. Qin, H. Yin, X. Du, W. Qin, X. Hao, *Energy Environ. Sci.* **2023**, *16*, 3350.
[44] B. Pang, C. Liao, X. Xu, S. Peng, J. Xia, Y. Guo, Y. Xie, Y. Chen, C. Duan, H. Wu, *Adv. Mater.* **2023**, *35*, 2211871.
[45] Y. Chen, R. Ma, T. Liu, Y. Xiao, H. K. Kim, J. Zhang, C. Ma, H. Sun, F. Bai, X. Guo, *Adv. Energy Mater.* **2021**, *11*, 2003777.
[46] S. Zhang, M. Cai, C. Shang, F. Bi, F. Feng, Z. Du, C. Sun, Y. Li, X. Bao, *Adv. Funct. Mater.* **2023**, *33*, 2301701.
[47] Y. Tamai, Y. Murata, S. i. Natsuda, Y. Sakamoto, *Adv. Energy Mater.* **2024**, *14*, 2301890.
[48] T. A. D. Peña, R. Ma, Z. Xing, Q. Wei, J. I. Khan, R. M. Young, Y. Hai, S. A. Garcia, X. Zou, Z. Jin, *Energy Environ. Sci.* **2023**, *16*, 3416.
[49] S.-i. Natsuda, T. Saito, R. Shirouchi, Y. Sakamoto, T. Takeyama, Y. Tamai, H. Ohkita, *Energy Environ. Sci.* **2022**, *15*, 1545.
[50] J. Rivnay, S. C. Mannsfeld, C. E. Miller, A. Salleo, M. F. Toney, *Chem. Rev.* **2012**, *112*, 5488.
[51] J. Cai, X. Zhang, C. Guo, Y. Zhuang, L. Wang, D. Li, D. Liu, T. Wang, *Adv. Funct. Mater.* **2021**, *31*, 2102189.
[52] D. He, J. Zhou, Y. Zhu, Y. Li, K. Wang, J. Li, J. Zhang, B. Li, Y. Lin, Y. He, C. Wang, F. Zhao, *Adv. Mater.* **2024**, *36*, 2308909.
[53] X. Liu, C. Zhang, C. Duan, M. Li, Z. Hu, J. Wang, F. Liu, N. Li, C. J. Brabec, R. A. Janssen, *J. Am. Chem. Soc.* **2018**, *140*, 8934.
[54] Y. Wang, D. Qian, Y. Cui, H. Zhang, J. Hou, K. Vandewal, T. Kirchartz, F. Gao, *Adv. Energy Mater.* **2018**, *8*, 1801352.
[55] J. Fu, Q. Yang, P. Huang, S. Chung, K. Cho, Z. Kan, H. Liu, X. Lu, Y. Lang, H. Lai, *Nat. Commun.* **2024**, *15*, 1830.
[56] J. Liu, S. Chen, D. Qian, B. Gautam, G. Yang, J. Zhao, J. Bergqvist, F. Zhang, W. Ma, H. Ade, *Nat. Energy* **2016**, *1*, 1.
[57] J. Fu, H. Chen, P. Huang, Q. Yu, H. Tang, S. Chen, S. Jung, K. Sun, C. Yang, S. Lu, *Nano Energy* **2021**, *84*, 105862.